Pergamon

Acta Materialia 50 (2002) 1717–1734

Acta MATERIALIA

www.actamat-journals.com

Grain-orientation-dependent residual stress and the effect of annealing in cold-rolled stainless steel

Y.D. Wang [a, c,*], R. Lin Peng [a, b], X.-L. Wang [c], R.L. McGreevy [a]

[a] *Studsvik Neutron Research Laboratory (NFL), Uppsala University, S-61182 Nyköping, Sweden*
[b] *Department of Mechanical Engineering, Linköping University, S-58183 Linköping, Sweden*
[c] *Spallation Neutron Source Project, Oak Ridge National Laboratory, Oak Ridge, TN 37831, USA*

Received 14 May 2001; received in revised form 20 December 2001; accepted 31 December 2001

Abstract

Cold rolling leads to a residual stress that is dependent not only on the specimen directions but also on the orientation of the grain. Neutron diffraction was used to investigate residual stresses and the effect of annealing in cold-rolled stainless steel, a two-phase material consisting of 62 vol% austenite and the rest deformation-induced martensite. The specimens were prepared by cold rolling of AISI 301 stainless steel with 48% reduction. The grain-orientation-dependent residual stress, or inter-granular stress, was determined by constructing the stress orientation distribution function, a recently developed concept, from the residual strains measured along various crystallographic directions. For the cold-rolled sample, a strong grain orientation anisotropy was observed for residual stresses in both phases. Detailed analysis of the experimental stress and texture data indicates that the observed orientation anisotropy was caused by the selective phase transformation that occurred during cold rolling. Annealing at 500°C leads to recovery, which significantly reduces the orientation anisotropy of the residual stress. The experimental data show that the recovery dynamics in the austenite and martensite phases are quite different. It appears that the overall recovery behavior in this two-phase material is driven by the martensite phase.

Keywords: Stress; Neutron scattering; Stainless steels; Texture; Phase transformations

1. Introduction

Understanding and control of residual stress is a prerequisite for the development and successful application of engineering materials in the aerospace, automotive and nuclear industries. Although residual stresses in a material come from many sources, in general they can be divided into three categories [1] according to their length scale:

1. Type I stress, which varies on a length scale of many grains (e.g., millimeters)
2. Type II stress (inter-granular stress), which varies from grain to grain
3. Type III stress, which originates from local defects and fluctuates within a grain

Traditionally, type I stress is also known as the *macrostress* while type II and type III stress are

* Corresponding author. Spallation Neutron Source Project, Oak Ridge National Laboratory, Oak Ridge, TN 37831, USA. Fax: +1-865-241-5177.
E-mail address: wangy@ornl.gov (Y.D. Wang).

1359-6454/02/$22.00
PII: S1359-6454(02)00021-6

collectively called the *microstress*. Type I stress by definition is independent of the orientation of individual grains. Type II stress, on the other hand, is grain orientation dependent. By this we mean that for a given stress component, the sign and magnitude of the type II stress within a grain is dependent on the orientation of the grain with respect to the specimen directions.

All three kinds of stresses can be determined experimentally. Amongst the techniques that are currently in use, X-ray and neutron diffraction provide an effective and non-destructive means for the determination of residual stress via the measurement of the shift and broadening of the diffraction peaks.

Normally, when diffraction is used to measure the *macro* residual stress in materials, a linear "d-spacing" vs $\sin^2\psi$ relationship is expected. However, for materials that have undergone large deformation, a so-called non-linear phenomenon, i.e., an oscillating "d-spacing" vs $\sin^2\psi$ distribution is often observed even in samples where the stress in the irradiated layers is known to be bi-aixal. The physical nature of this non-linear behavior has been mainly attributed to two factors: the influence of crystallographic texture on the diffraction elastic constants [2,3] and the existence of type II stress [4,5] which is grain orientation dependent. In the past, interpretation of such data has been focused on the influence of crystallographic texture by incorporating the crystallographic orientation distribution function (CODF) into a proper mechanical model. Indeed, there has been some success in modeling the observed non-linear dependence using the Reuss (uniform stress), Voigt (uniform strain), Hill (average model), or other phenomenological models [6,7]. However, a large discrepancy between the measured and calculated strains is still observed in materials where the grain-orientation-dependent residual stress is significant [8]. For these materials, an unambiguous assessment of the macro residual stress can be obtained only by including the grain-orientation-dependent type II stress.

The inter-granular or type II stress in polycrystalline materials is caused by stress or strain incompatibility between grains having different crystallographic orientations during mechanical or thermo-mechanical deformation. Thus, a study of the grain orientation dependence of the residual stress not only enables an unambiguous assessment of the macro residual stress but also helps to answer fundamental questions such as how the grain-to-grain interactions occur in a polycrystalline material during and after deformation. Furthermore, investigations of the grain orientation dependence provide valuable information concerning the history of thermo-mechanical treatment in engineering materials. For this reason, much attention has been paid to the study of the grain-orientation-dependent residual stress in the past few years [9–13]. Theoretical work in this area has mainly been carried out using 3D crystallographic plasticity simulations, in which the stress states of individual grains are modeled by considering the physical mechanisms that produce the residual stress during plastic and/or elastic deformation. These numerical methods include the Taylor model [9], the self-consistent models [10–12], and the finite element method [13]. However, while these models are able to produce a qualitative description of the stress states in individual grains with different orientations, the calculated strains sometimes differ from the experimental values by more than 30% [12], especially for samples subjected to a large degree of plastic deformation. In materials where phase transformation occurs during deformation [14], additional inter-granular stress is generated due to the transformation. The transformation-induced intergranular stress becomes particularly complex when the transformation is selective with respect to the crystallographic axes [15]. Thus, despite the progress in recent years, quantitative simulation of the deformation behaviors, particularly the stress or strain state of individual grains, in polycrystalline aggregates is far from being satisfactory, even for cubic materials [16].

Direct measurements of the stress state in individual grains are becoming possible [17–21]. For example, using high-energy X-ray beams at synchrotron sources, the evolution of the grain orientation and stress state during deformation has been demonstrated for individual grains [17,18]. However, in order to determine the properties of polycrystalline aggregates, a statistical representation of all grains is still needed. Despite recent

advances in synchrotron techniques, mapping out a large number of grains within a bulk specimen remains a technological challenge.

On the other hand, X-ray or neutron diffraction measurements over a finite sampling volume give a statistical representation of the grain-orientation-dependent strain or stress. Initial attempts to estimate the grain-orientation-dependent strain or stress can be traced back to the measurements of strain pole figures [22,23] using X-ray or neutron diffraction. Recently, a new method was developed for experimental evaluation of the grain-orientation-dependent residual stress in polycrystalline materials. Analogous to texture representation by the CODF, the concept of stress orientation distribution function (SODF) [24–26] was introduced, which describes the grain-orientation-dependent residual stress as a mean stress field in the Euler orientation space. It should be noted that the SODF defined here belongs to the generalized textural quantities proposed by Bunge [27].

Previous studies [24–26] have established that just like the CODF, the SODF may be constructed using the Spherical Harmonic Analysis (SHA) method, where the mean stress field, expressed as a second-rank tensor, is expanded in terms of generalized spherical harmonics whose series coefficients are determined directly from the measured lattice strains along various specimen directions. As will be seen below, this method is naturally adapted to textured materials, thereby allowing the influence of texture on the diffraction elastic constants and the existence of type II stress to be considered simultaneously. The stress and strain equilibrium between neighbouring grains is considered by implementing a self-consistent model in an iterative algorithm, which reduces the number of strain measurements required for the construction of the SODF. Once the SODF is constructed, the stress tensor for a given texture component may be calculated.

In this paper, the SHA method was used to investigate the grain-orientation-dependent residual stress in a cold-rolled stainless steel, prior to and after annealing. The material consists of two phases, namely the austenite (γ) and deformation-induced martensite (α). A previous study by neutron diffraction revealed a large inter-granular or type II stress in the cold-rolled condition, so that the residual stress within a grain is highly dependent on the orientation of the grain [8]. It has been suggested that for heavily deformed materials, the grain-orientation-dependent residual stress may play an important role in determining the recrystallization texture [28]. In this two-phase material, the grain-orientation-dependent residual stress may also have a strong influence on the transformation texture by either preventing or promoting the growth of grains with certain orientation [15]. Thus, experimental investigations on the correlation between the residual stress and the grain orientation in this two-phase material not only shed light on the interactions between grains, but also provide valuable information for modeling the variant selections during phase transformation and the nucleation and growth of new grains during recrystallization. In addition, measurements of stress relaxation in the annealed state will elucidate the recovery behaviors in each phase.

2. Experimental details

2.1. Material

A commercial stainless steel, equivalent to AISI 301 with a nominal chemical composition of 17 wt% Cr and 7 wt% Ni (remainder Fe), was used in this study. The as-received material was 0.8 mm thick sheets which were obtained from 1.538 mm thick sheets by three-pass cold rolling (48% reduction). The yield and ultimate tensile strength of the as-received material are 1408 and 1500 MPa, respectively. Neutron diffraction measurements show that the cold-rolled material consists of austenite with a fcc lattice and deformation-induced martensite with a bcc lattice. The volume fraction of the martensite, estimated by analyzing the peak intensities of $(1\,1\,1)_\gamma$, $(2\,0\,0)_\gamma$, $(2\,2\,0)_\gamma$, $(3\,1\,1)_\gamma$, $(1\,1\,0)_\alpha$, $(2\,0\,0)_\alpha$ and $(2\,1\,1)_\alpha$, is $\sim$ 38%. To investigate the effect of recovery on the residual stress, a sample was also annealed at 500°C in air for 2 h and then furnace cooled to room temperature. The optical microstructures obtained for this sample showed no evidence of recrystallization in either phase.

2.2. Sample preparation

For the as-rolled condition, cylindrical specimens were prepared. The specimens were made by first spark erosion cutting the cold-rolled sheets into discs with a diameter of 8 mm. These discs were then stacked together, with their rolling direction (RD) carefully aligned, to form a cylindrical specimen of 12 mm high with the axis of the cylinder parallel to the normal direction (ND). For the annealed condition, a spherical specimen was prepared. This specimen was made by first cutting the cold-rolled sheets into discs of various sizes, which were then carefully aligned and stacked together to form a pseudo sphere. The diameter of the sphere is approximately 12 mm. Fig. 1 shows the specimen and crystallographic coordinate systems used for the definition of various directions and angles.

2.3. Strain measurements

The neutron diffraction strain measurements were carried out using the high-resolution diffractometer, REST, at the Studsvik Neutron Research Laboratory in Sweden. The nominal wavelength of the neutron beam is 1.76 Å. For the cold-rolled sample, the lattice strains were measured using the $(2\,0\,0)_\gamma$, $(2\,2\,0)_\gamma$, $(3\,1\,1)_\gamma$, $(2\,0\,0)_\alpha$ and $(2\,1\,1)_\alpha$ reflections. The elastic strain distributions were determined at 10° intervals in the γ phase and 5° intervals in the α phase in the three planes formed by RD, TD, and ND. For the annealed sample, lattice strains for $(2\,0\,0)_\gamma$, $(2\,2\,0)_\gamma$, $(3\,1\,1)_\gamma$, $(2\,0\,0)_\alpha$ and $(2\,1\,1)_\alpha$ were determined over a $10° \times 10°$ grid using an Euler cradle attached on REST, with the same set-up as in a texture measurement. Following the convention of Brakman [2], the elastic strain distributions obtained in this set-up are referred to as the strain pole figure, which is analogous to the intensity pole figure, which describes the distribution of the diffraction intensity for a given reflection along various specimen directions.

Powder-like γ phase material was extracted by dissolving the α phase with a 1 M H_2SO_4 + 0.2 M NaCl solution and used as a stress-free sample to determine the d_0 value for the γ phase. Because a stress-free sample for the α phase was rather difficult to obtain, the d_0 value for the α phase was derived by imposing the condition of static equilibrium between the α and γ phases, i.e.,

$$f_\gamma \sigma_\gamma + f_\alpha \sigma_\alpha = 0 \tag{1}$$

where f_γ and f_α are, respectively, the volume fraction of the γ and α phases. σ_γ and σ_α are the orientation independent part of the stress in each phase, usually denoted as the phase-stress. Note that the macro (type I) stress is not a concern here, since

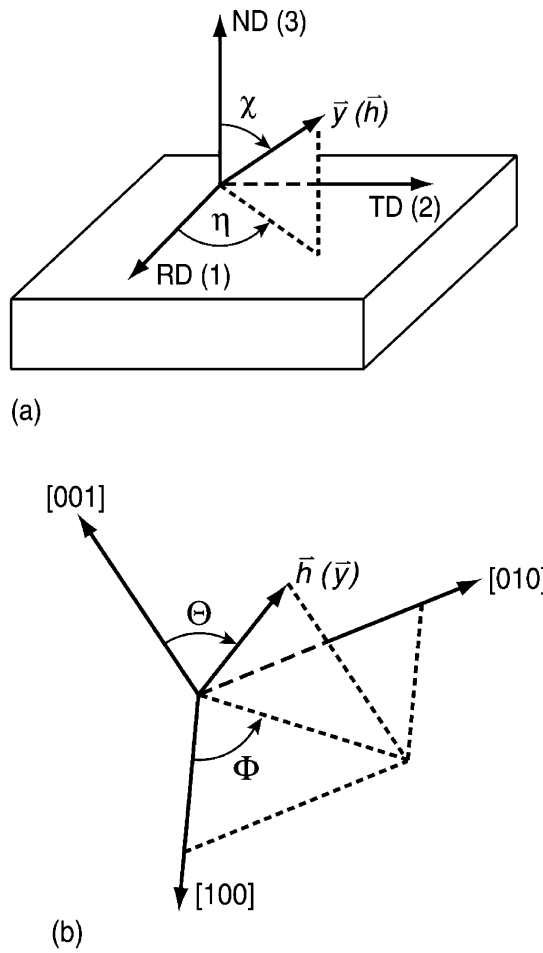

Fig. 1. Specimen and crystallographic coordinate systems used for the definition of various directions and angles: (a) sample coordinate system; (b) crystal coordinate system. RD: rolling direction. TD: transverse direction. ND: normal direction. χ and η are the polar and azimuthal angles in the specimen coordinate system. Θ and Φ are the polar and azimuthal angles in the crystallographic coordinate system.

the specimens were always fully illuminated by the neutron beam in all measurement geometries.

2.4. Texture measurements

The neutron diffraction texture measurements were also carried out on REST. Three complete pole figures were obtained for the γ phase, using the $(2\,0\,0)_\gamma$, $(2\,2\,0)_\gamma$ and $(3\,1\,1)_\gamma$ reflections. For the α phase, two complete pole figures were obtained using the $(2\,0\,0)_\alpha$ and $(2\,1\,1)_\alpha$ reflections. In order to investigate possible texture gradients, partial pole figures (up to $\chi_f = 70°$) were measured in the surface layer of the samples using a Seifert PTS 3000 diffractometer with Co K_α radiation. The ODF analysis was carried out using the modified maximum entropy method [29] from the experimental pole figures.

3. Textures and strain distributions

3.1. Textures

The $(2\,0\,0)_\gamma$, $(2\,2\,0)_\gamma$ and $(3\,1\,1)_\gamma$ pole figures for the γ phase, measured by neutron diffraction, are shown in Fig. 2 for the cold-rolled sample. Orthorhombic sample symmetry was observed in all three pole figures, which not only conveniently reduces the strain measurements from a full strain pole figure to a quadrant, but also reduces the number of series coefficients required for the complete description of the SODF. The pole figures measured by X-ray diffraction in the surface layer of the cold-rolled sheet are almost identical to those measured by neutron diffraction, indicating little texture gradient through the thickness. This observation is further confirmed by the corresponding ODF cross-sections at constant φ, which are shown in Fig. 3 for the bulk and surface layer of the sample, respectively. Texture in the γ phase consists of mainly the $\{1\,1\,0\}\langle 2\,1\,1\rangle$ (brass), $\{1\,1\,0\}\langle 0\,0\,1\rangle$ (Goss), $\{123\}\langle 634\rangle$ (S) and $\{1\,1\,2\}\langle 1\,1\,1\rangle$ (copper) components. These are all typical texture components found in cold-rolled stainless steel [14].

The $(2\,0\,0)_\alpha$ and $(2\,1\,1)_\alpha$ pole figures for the α phase are shown in Fig. 4. As it can be seen, the

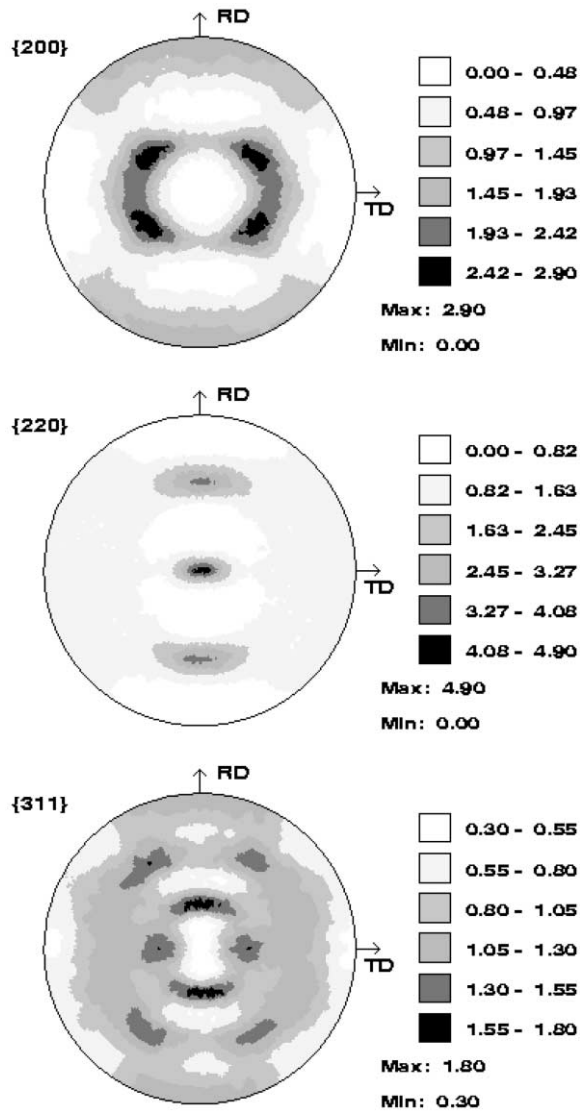

Fig. 2. $(2\,0\,0)_\gamma$, $(2\,2\,0)_\gamma$ and $(3\,1\,1)_\gamma$ pole figures of the γ phase in cold-rolled stainless steel measured by neutron diffraction.

pole figures for the α phase also display orthorhombic sample symmetry, with slightly weaker texture intensity than that in the γ phase. The derived ODF cross-sections are shown in Fig. 5, which indicates that the texture in the α phase consists of mainly the $\{332\}\langle 113\rangle$, $\{1\,1\,2\}\langle 131\rangle$ components and a component running from $\{2\,1\,1\}\langle 011\rangle$ to $\{100\}\langle 011\rangle$ (i.e., the $\langle 011\rangle$//RD fiber). These observations are consistent with the

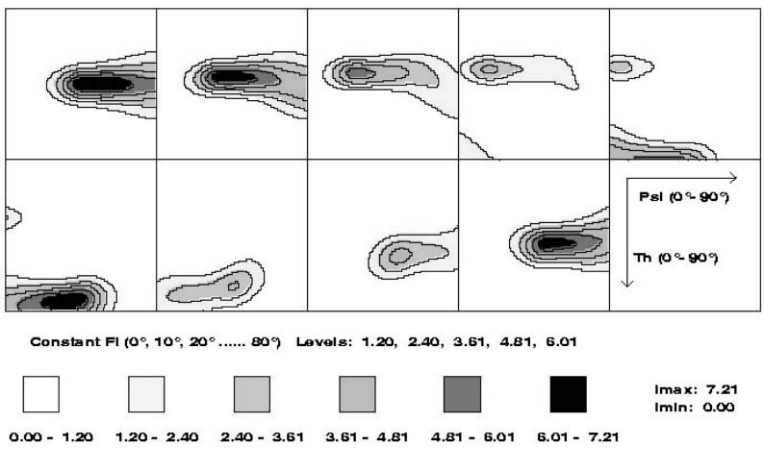

(a)

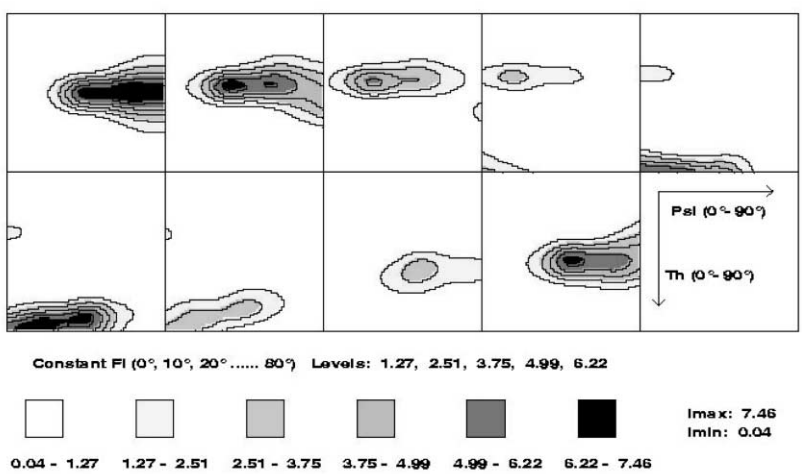

(b)

Fig. 3. ODF sections with φ constant (0°, 10°, …, 90°) in the (a) bulk sample and (b) surface layer of the γ phase in cold-rolled stainless steel. Data in (a) were obtained with neutron diffraction and those in (b) with X-ray diffraction.

transformation texture from γ to α found in stainless steel [14], which will be discussed in greater detail below.

3.2. Strains

The strain pole figures for the α and γ phases are shown in Figs. 6 and 7, respectively. The left panel of each figure is for the cold-rolled condition, while the right panel is for the annealed condition. In the cold-rolled state, for both phases, the strains obtained with different reflections differ not only in absolute values but also in the overall strain pole figure pattern. The variation of absolute strain values for different *hkl*-planes may be attributed to the influence of texture. However, the discrepancy among the strain pole figure patterns is a clear indication of the presence of the inter-granular stress, or orientation anisotropy in residual stress.

The effect of annealing is apparent by comparing the strain pole figures obtained in the cold-rolled and annealed conditions, respectively. For both phases, annealing at 500°C drastically reduces the orientation anisotropy of residual stress. For the α phase, in particular, the anisotropy in residual stress vanishes, as demonstrated by the similarity

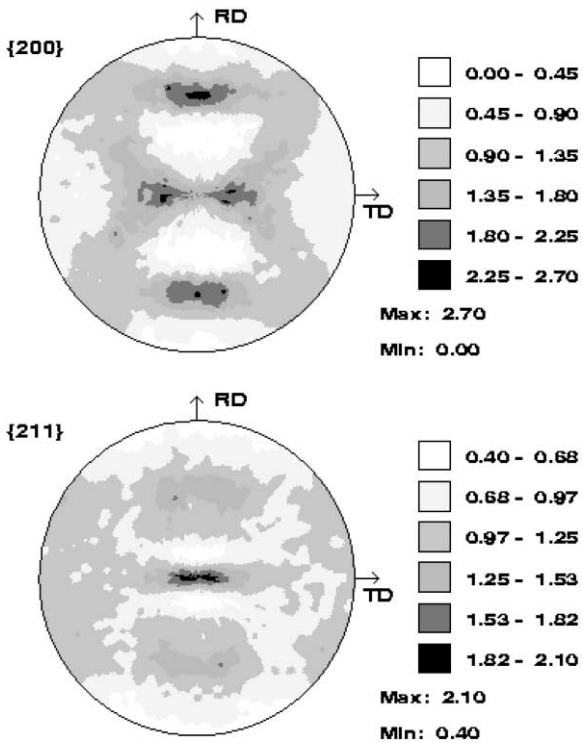

Fig. 4. $(2\,0\,0)_\alpha$ and $(2\,1\,1)_\alpha$ pole figures of the α phase measured by neutron diffraction.

between the $(2\,0\,0)_\alpha$ and $(2\,1\,1)_\alpha$ strain pole figures. To further illustrate the effect of annealing, line scans along ND–TD are shown in Figs. 8 and 9 for γ and α phases, respectively. For the γ phase, the strains measured with $(2\,0\,0)_\gamma$, $(2\,2\,0)_\gamma$ and $(3\,1\,1)_\gamma$ still differ, but the difference is much smaller than in the cold-rolled condition. For the α phase, the strains measured with $(2\,0\,0)_\alpha$ and $(2\,1\,1)_\alpha$ overlap after annealing. As will be explained later, the difference in the change of orientation anisotropy observed here was due to the different recovery dynamics in the γ and α phases. Note that both the $(3\,1\,1)_\gamma$ and $(2\,1\,1)_\alpha$ reflections, which are traditionally used for stress determination with X-ray and neutron diffraction, are affected by the grain-orientation-dependent residual stress. As it can be seen from Figs. 8 and 9, the $(3\,1\,1)_\gamma$ and $(2\,1\,1)_\alpha$ strains do not vary monotonously with the title angle, as would have been expected if the inter-granular stress were absent. This result means that for heavily deformed materials, in which the inter-granular stress is significant, the $(3\,1\,1)_\gamma$ and $(2\,1\,1)_\alpha$ reflections do not necessarily provide a reliable measure of the *macro* residual stress [24].

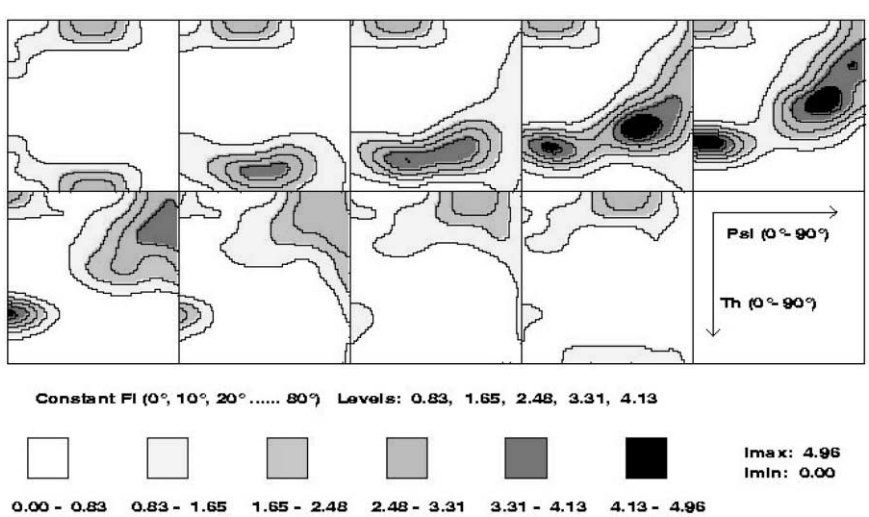

Fig. 5. ODF sections with φ constant (0°, 10°, …, 90°) in the bulk sample of the α phase in cold-rolled stainless steel.

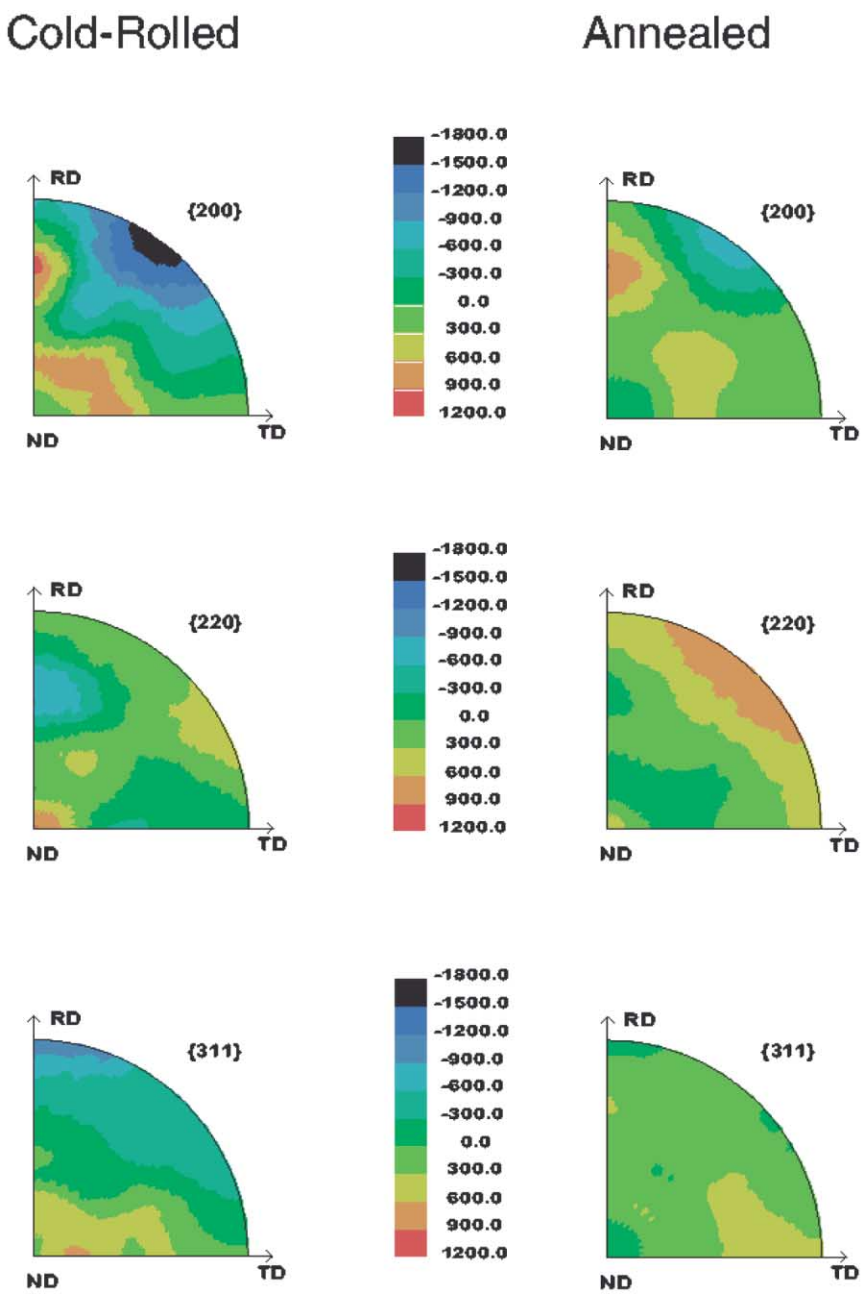

Fig. 6. Strain pole figures in the γ phase. Left panel: cold-rolled condition. Right panel: annealed condition.

4. Quantitative analysis of residual stress

The experimental results presented in Figs. 6–9 are for residual strains. As stated earlier, due to the presence of the inter-granular stress, the residual stress cannot be calculated from the measured residual strains in the conventional way. In the following, the spherical harmonic approach is applied to determine the residual stress via the construction of SODF.

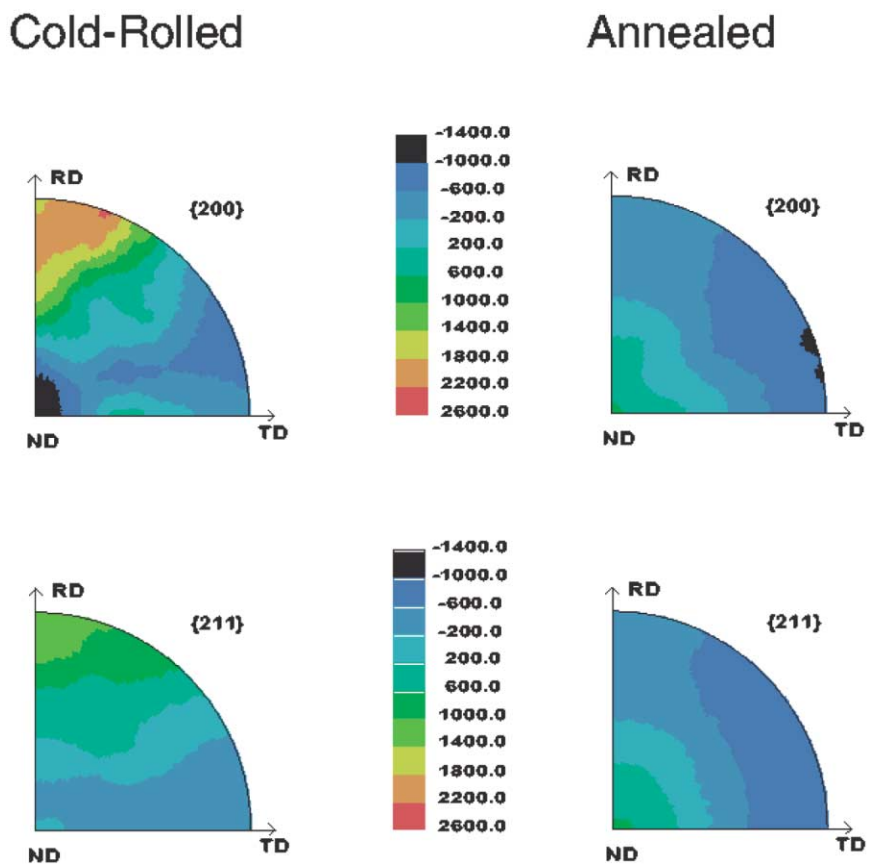

Fig. 7. Strain pole figures in the α phase. Left panel: cold-rolled condition. Right panel: annealed condition.

4.1. Analysis method

Since details of this analysis method has been described elsewhere [30], only an outline is given here. Similar to the CODF [31,32], the SODF, $\sigma_{ij}(g)$, can be expressed in terms of generalized spherical harmonics, i.e.,

$$\sigma_{ij}(g) = \sum_{l=0}^{L^S_{\max}} \sum_{m=-l}^{l} \sum_{n=-l}^{l} \Gamma^{ij}_{lmn} Z_{lmn}(\cos\theta) \exp(-im\psi)\exp(-in\varphi) \quad (2)$$

where g describes the SO3 rotation group in the Euler orientation space, Γ^{ij}_{lmn} are the series coefficients of the SODF, $Z_{lmn}(x)$ is the augmented Jacobi function, $(\psi\theta\varphi)$ are Euler angles defined in Roe's notation [32], and $L^S_{\max}$ is the maximum order of series coefficients in the SODF. The specimen and crystallographic coordinate systems used for the definition of various directions and angles are illustrated in Fig. 1.

For a textured material, the lattice strain $\tilde{\varepsilon}(\vec{h},\vec{y})$ measured with diffraction plane $\vec{h}$ in sample direction $\vec{y}$ is given by

$$\tilde{\varepsilon}(\vec{h},\vec{y}) = \frac{\oint_{g\in\vec{y}//\vec{h}} f(g)\varepsilon(\vec{y},g)\mathrm{d}g}{\oint_{g\in\vec{y}//\vec{h}} f(g)\mathrm{d}g} \quad (3)$$

where $f(g)$ is the crystal orientation distribution function (ODF), which may be expressed as

$$f(g) = \sum_{l=0}^{L^C_{\max}} \sum_{m=-l}^{l} \sum_{n=-l}^{l} W_{lmn} Z_{lmn}(\cos\theta) \quad (4)$$

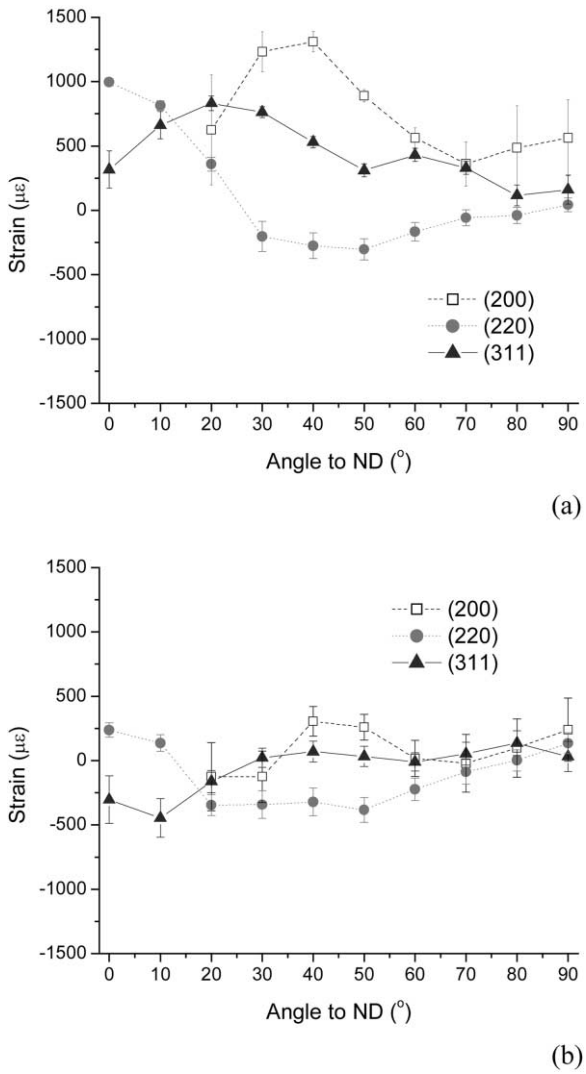

Fig. 8. Strain distributions along the ND–TD line in the γ phase: (a) cold-rolled condition; (b) annealed conditions.

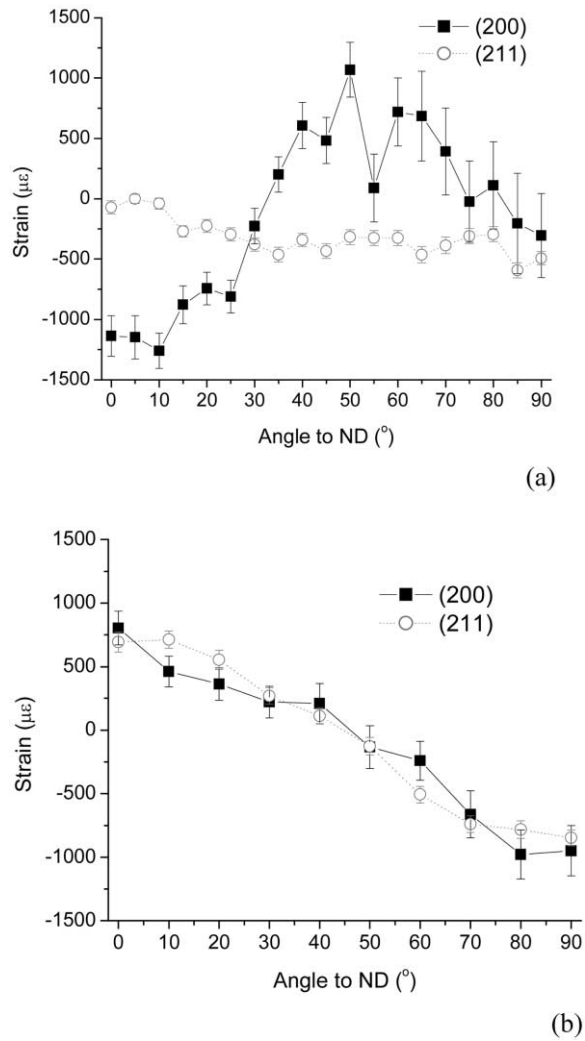

Fig. 9. Strain distributions along the ND–TD line in the α phase: (a) cold-rolled condition; (b) annealed conditions.

$$\exp(-im\psi)\exp(-in\varphi)$$

Here, the W_{lmn} are the series coefficients and $L_{\max}^{C}$ is the maximum order of series coefficients in the ODF.

According to the generalized Hooke's law, the elastic strain $\varepsilon_{ij}(g)$ is related to $\sigma_{ij}(g)$ by

$$\varepsilon_{ij}(g) = S_{ijkl}(g)\sigma_{kl}(g) \tag{5}$$

where $S_{ijkl}(g)$ is the elastic compliance which may be expressed as irreducible spherical tensors, i.e.,

$$S_{ijkl}(g) = \sum_{l=0}^{4}\sum_{m=-l}^{l}\sum_{n=-l}^{l} e_{lmn}^{ijkl} Z_{lmn}(\cos\theta) \exp(-im\psi)\exp(-in\varphi) \tag{6}$$

where e_{lmn}^{ijkl} are the series coefficients of the elastic compliance of a single crystallite.

Introducing (2), (4), (5) and (6) into the integral equation (3), the lattice strain $\tilde{\varepsilon}(\vec{h},\vec{y})$ for a crystallite with $\vec{h}//\vec{y}$ may be written as

$$\tilde{\varepsilon}(\vec{h},\vec{y}) = \sum_{i=1}^{3}\sum_{j=1}^{3}\sum_{l=0}^{L'_{\max}}\sum_{m=-l}^{l}\sum_{n=-l}^{l}\alpha_i\alpha_j q Q^{ij}_{lmn} P_l^m(\cos\chi) \quad (7)$$
$$\exp(-im\eta)P_l^n(\cos\Theta)\exp(in\Phi)$$

with

$$Q^{kl}_{lmn} = \sum_{l=|l_2-l_1|}^{|l_2+l_1|}\sum_{l_2=|l_3-l_4|}^{|l_3+l_4|}(l_1l_2m_1m_2|lm)(l_1l_2n_1n_2|ln)(l_3l_4m_3m_4|l_2m_2)(l_3l_4n_3n_4|l_2n_2)W_{l_1m_1n_1}\ \Gamma^{ij}_{l_3m_3n_3}\ e^{klij}_{l_4m_4n_4} \quad (8)$$

$$q^{-1} = \sum_{l=0}^{L_{\max}}\sum_{m=-l}^{l}\sum_{n=-l}^{l} W_{lmn}P_l^m(\cos\chi) \quad (9)$$
$$\exp(-im\eta)P_l^n(\cos\Theta)\exp(in\Phi)$$

where (Θ,Φ) are the polar and azimuthal angles of $\vec{h}$ in the crystal co-ordinate system; χ and η are the polar and azimuthal angles of $\vec{y}$ in the sample co-ordinate system; α_i is the direction cosine of (χ,η) in the ith direction; $P_l^m(x)$ is the Legendre function; $L'_{\max}$ is the maximum order of series coefficients determined by the combined production of three harmonics; the term $(l_1l_2m_1m_2|lm)$ denotes the Clebsch–Gordan coefficients. It is easy to see from (7) to (9) that a linear relationship exists between $\tilde{\varepsilon}(\vec{h},\vec{y})$ and Γ^{ij}_{lmn}, which has allowed a limited number of series coefficients of SODFs to be determined from the measured lattice strains.

The condition of stress or strain equilibrium between neighboring grains is considered by implementing the Eshelby's "inclusion" model [33] in the SODF analysis. The optimal solution of the SODF is determined by an algorithm that solves a non-linear optimization problem by minimizing both the errors between the calculated and measured lattice strains and between the misfit of the real state of stress and the self-consistent state for all grains [30].

The single crystal elastic constants used in the model are as follows:

C_{11} = 204.6 GPa, C_{12} = 137.7 GPa, and C_{44} = 126.2 GPa for the γ phase;
C_{11} = 236.9 GPa, C_{12} = 140.6 GPa, and C_{44} = 116.0 GPa for the α phase.

The former is taken from the single crystal elastic constants obtained for stainless steel of a similar chemical composition [34] while the latter from the single crystal elastic constants obtained for pure bcc iron [35]. For the self-consistent model, each α or γ grain is treated as an ellipsoidal inclusion with an aspect ratio of 5:2:1 for RD:TD:ND. The Eshelby tensor for an inclusion of arbitrary ellipsoidal shape embedded in an elastically anisotropic polycrystal is calculated by a numerical method [16]. The anisotropic medium is assumed to be a homogenous mixture of α and γ with the volume fraction specified previously.

4.2. Analysis results

Tables 1–4 give in detail the stress tensor calculated for major texture components in the γ and α phases, respectively. The second last line in each table gives the phase-stress which is orientation independent. The errors for these calculated stresses are estimated to be less than $\pm$ 20 MPa for main texture components. The $\pm$ sign in the shear stress component means that the effect of sample and crystal symmetry on the SODF leads to the existence of a pair of shear stresses with opposite signs for grains having those symmetry orientations. The influence of the crystal symmetry on the SODF has been discussed previously [25].

As a crude measure of the grain orientation dependence of the residual stress, an orientation anisotropy factor is introduced which is defined as

$$\Delta_{ij} = \frac{\oint(\sigma_{ij}(g)-\sigma_{ij})^2 dg}{\sum_k \sigma_{kk}^2} \quad (10)$$

where σ_{ij} is the phase-stress. In the absence of grain orientation anisotropy, $\Delta_{ij} = 0$. The sum $\oint(\sigma_{ij}(g)-\sigma_{ij})^2 dg$ is similar to the texture index used in the texture analysis. Normalizing $\oint(\sigma_{ij}(g)-\sigma_{ij})^2 dg$ by $\sum_k \sigma_{kk}^2$ allows a comparison to be made for the anisotropy factors in different phases and

Table 1
Stress tensor for major texture components in the austenite phase of cold-rolled stainless steel

Texture components	Euler angle ψ,θ,φ	σ_{11} (MPa)	σ_{22} (MPa)	σ_{33} (MPa)	σ_{23} (MPa)	σ_{13} (MPa)	σ_{12} (MPa)
{1 1 0}⟨1 1 2⟩ (B)	(54.74°, 45°, 0°)	−292	37	73	0	0	±13
{1 1 0}⟨0 0 1⟩ (G)	(90°, 45°, 45°)	9	64	158	0	0	0
{1 1 2}⟨1 1 1⟩ (C)	(0°, 35.3°, 45°)	−188	−83	−108	0	±41	0
{1 2 3}⟨6 3 4⟩ (S)	(31°, 36.7°, 26.6°)	−250	12	5	±24	±30	0
Phase-stress	—	−113	8	46	0	0	0
Anisotropy factor, Δ_{ij}		4.8	0.8	2.6	0.0	0.2	0.0

Table 2
Stress tensor for major texture components in the austenite phase of cold-rolled stainless steel followed by annealing at 500°C

Texture components	Euler angle $\{\psi,\theta,\varphi\}$	σ_{11} (MPa)	σ_{22} (MPa)	σ_{33} (MPa)	σ_{23} (MPa)	σ_{13} (MPa)	σ_{12} (MPa)
{1 1 0}⟨1 1 2⟩ (B)	(54.74°, 45°, 0°)	65	142	70	0	0	±86
{1 1 0}⟨0 0 1⟩ (G)	(90°, 45°, 45°)	160	196	206	0	0	0
{1 1 2}⟨1 1 1⟩ (C)	(0°, 35.3°, 45°)	66	174	−36	0	±62	0
{1 2 3}⟨6 3 4⟩ (S)	(31°, 36.7°, 26.6°)	60	153	−10	±4	±34	±34
Phase-stress	—	115	130	37	0	0	0
Anisotropy factor, Δ_{ij}		0.3	0.2	1.2	0.0	0.2	0.3

Table 3
Stress tensor for major texture components in the martensite phase of cold-rolled stainless steel

Texture components	Euler angle $\{\psi,\theta,\varphi\}$	σ_{11} (MPa)	σ_{22} (MPa)	σ_{33} (MPa)	σ_{23} (MPa)	σ_{13} (MPa)	σ_{12} (MPa)
{3 3 2}⟨1 1 3⟩	(0°, 64.76°, 45°)	303	−105	49	0	±19	0
{1 1 1}⟨1 1 2⟩	(0°, 54.74°, 45°)	324	−146	30	0	±14	0
{0 0 1}⟨1 1 0⟩	(90°, 0°, 45°)	−262	−40	−223	0	0	0
{1 1 3}⟨1 1 0⟩	(90°, 25°, 45°)	43	−25	21	±6	0	0
{1 1 2}⟨1 1 0⟩	(90°, 30°, 45°)	125	15	75	±38	0	0
{1 1 1}⟨1 1 0⟩	(90°, 54.75°, 45°)	135	161	24	±63	0	0
{1 1 2}⟨1 3 1⟩	(58.52°, 30°, 45°)	237	−118	33	±60	±11	±6
Phase-stress	—	185	−43	−35	0	0	0
Anisotropy factor, Δ_{ij}		7.0	1.8	1.9	0.2	0.0	0.0

Table 4
Stress tensor for major texture components in the martensite phase of cold-rolled stainless steel followed by annealing at 500°C

Texture components	Euler angle $\{\psi,\theta,\varphi\}$	σ_{11} (MPa)	σ_{22} (MPa)	σ_{33} (MPa)	σ_{23} (MPa)	σ_{13} (MPa)	σ_{12} (MPa)
$\{3\,3\,2\}\langle 1\,1\,3\rangle$	(0°, 64.76°, 45°)	−242	−349	64	0	±6	0
$\{1\,1\,1\}\langle 1\,1\,2\rangle$	(0°, 54.74°, 45°)	−283	−377	47	0	±29	0
$\{0\,0\,1\}\langle 1\,1\,0\rangle$	(90°, 0°, 45°)	−250	−218	−68	0	0	0
$\{1\,1\,3\}\langle 1\,1\,0\rangle$	(90°, 25°, 45°)	−211	−216	8	±43	0	0
$\{1\,1\,2\}\langle 1\,1\,0\rangle$	(90°, 30°, 45°)	−212	−234	23	±34	0	0
$\{1\,1\,1\}\langle 1\,1\,0\rangle$	(90°, 54.75°, 45°)	−252	−289	50	±23	0	0
$\{1\,1\,2\}\langle 1\,3\,1\rangle$	(58.52°, 30°, 45°)	−208	−267	21	±74	±45	0
Phase-stress	—	−205	−252	10	0	0	0
Anisotropy factor, Δ_{ij}		0.1	0.3	0.1	0.1	0.0	0.0

between the cold-rolled and annealed conditions. The calculated values of Δ_{ij} are listed at the bottom of each table.

5. Discussion

5.1. Texture and residual stress in cold rolled stainless steel

The residual stress in the cold-rolled condition exhibits strong orientation dependence. This can be readily seen by examining the calculated stress tensor for major texture components. In the γ phase, for example, the brass component ($\{1\,1\,0\}\langle 2\,1\,1\rangle$) shows a large compressive stress of −292 MPa along the rolling direction whereas the Goss component ($\{1\,1\,0\}\langle 0\,0\,1\rangle$) is almost stress free in the same direction. Similarly, strong orientation dependence is also seen in the α phase. Comparison of Δ_{ij} values in Tables 1 and 3 indicates that the orientation anisotropy of residual stress in the α phase is somewhat larger than that in the γ phase. This is consistent with the anisotropy observed in measured residual strains (see Figs. 8 and 9). For a given sample direction, the residual stresses in the α phase vary from tension to compression, with the largest difference found between the $\{1\,1\,1\}\langle 1\,1\,2\rangle$ and $\{0\,0\,1\}\langle 1\,1\,0\rangle$ texture components, which is about 560 MPa in the rolling direction.

Note that the phase-stress in each phase is not hydrostatic. Upon annealing, the phase-stresses in both phases become almost bi-axial. The multi-axial phase-stress observed for the cold-rolled sample is consistent with the $\gamma\rightarrow\alpha$ phase transformation that occurred during cold rolling. The $\gamma\rightarrow\alpha$ transformation led to the appearance of the martensite α phase, which is hard and exhibits much larger yield strength than the γ phase. Upon further tensile deformation by cold rolling, both phases are deformed plastically. However, the degrees of plastic deformation in the two phases are different due to the large differences in yield strength. The softer γ phase yields early and shows a much larger plastic strain. As a result, when the loading force is removed, the γ phase is put into compression while the α phase is in tension in the rolling direction.

The characteristic texture seen in the cold-rolled sample is also consistent with the picture of $\gamma\rightarrow\alpha$ transformation. The textures of both the austenite and martensite phases in cold-rolled stainless steel have been investigated thoroughly by Raabe [14]. A very interesting phenomenon observed by him is that at large reduction, the brass orientation in the γ phase is no longer the dominant component but is accompanied by a Goss orientation. The texture obtained for our cold-rolled specimen (with 48% reduction) is consistent with his results for 50–60% cold-rolled stainless steel, where the brass and Goss orientations are of comparable densities.

The formation of additional Goss component in the γ phase was attributed to the selective phase transformation, i.e., the $\gamma\rightarrow\alpha$ transformation during cold rolling was selective with respect to orien-

tation of the austenite crystallite (relative to the sample coordinates). In a previous study of the martensitic phase transformation in textured, austenitic stainless steel, Goodchild et al. [15] observed that after tensile deformation in the unstable temperature region, martensite is formed in all grains except in those extended along $\langle 0\,0\,1\rangle$. Conversely, compressive deformation caused transformation in grains compressed along $\langle 0\,0\,1\rangle$ but not in grains in which the compression axis was close to $\langle 011\rangle$. Based on these observations and his own investigations, Raabe [14] concluded that the Goss component ($\{1\,1\,0\}\langle 0\,0\,1\rangle$) is stable during cold-rolling since it has a $\langle 0\,0\,1\rangle$ direction parallel to the tensile axis (RD) and a $\langle 1\,1\,0\rangle$ direction parallel to the compression axis (ND). On the other hand, the brass component ($\{1\,1\,0\}\langle 1\,1\,2\rangle$) is less stable because it reveals a $\langle 1\,1\,0\rangle$ direction parallel to the ND, but no $\langle 100\rangle$ direction parallel to the RD. Rabbe [14] further pointed out that the new texture component in the martensite α phase should exhibit a strict crystallographic relationship to the brass component in the austenite γ phase. Using the Nishiyama–Wassermann (N–W) transformation rule, he derived a strict crystallographic relationship between the brass component in γ and a $\{332\}\langle 113\rangle$ component in α. Indeed, our measurements with 48% cold-rolled stainless steel show that major texture components in the martensite phase are located around the $\{332\}\langle 113\rangle$, with a few grains rotating to $\{1\,1\,1\}\langle 1\,1\,2\rangle$.

The intergranular stresses reported in Tables 1 and 3 provided further evidence of the selective transformation in stainless steel during deformation by cold rolling.

1. The σ_{11} of the brass ($\{1\,1\,1\}\langle 1\,1\,2\rangle$) component in the austenite shows the same signs as that of its phase stress, but with far greater magnitude. This indicates that the brass component is in a relatively advanced stage of transformation. Similar results can be seen for the $\{3\,3\,2\}\langle 1\,1\,3\rangle$ texture component in the martensite. Furthermore, the σ_{22} for the brass and the $\{3\,3\,2\}\langle 1\,1\,3\rangle$ components also matched well. All these experimental observations are consistent with a selective transformation led by $\{1\,1\,1\}\langle 1\,1\,2\rangle \rightarrow \{3\,3\,2\}\langle 1\,1\,3\rangle$.
2. As shown in Tables 1 and 2, the inter-granular stress of the Goss component exhibits no apparent correlation with the phase stress of the γ phase, or with the inter-granular stress of a major texture component in the α phase. It can be seen, therefore, that the Goss component was relatively stable during the transformation.

5.2. On stress analysis and simulations based on 3D crystallographic plasticity

Investigations of the inter-granular stresses in stainless steel have been reported in several publications [12,36,37], including in-situ neutron diffraction measurements of samples subjected to uniaxial tensile load. The main purpose of those papers was to study the diffraction strain responses for different *hkl*-planes and compare the results with those predicted by numerical models, mostly the elastic–plastic self-consistent (EPSC) model [10,38]. It has been shown that for a small degree of elastic and/or plastic deformation, this model is capable to qualitatively describe the evolution of lattice strains. However, for certain *hkl*-planes, the lattice strains calculated by the model disagree with experimental results by more than 30% [12,37].

For polycrystalline materials subjected to moderate to large plastic deformation, such as the cold-rolled steel investigated in this paper, the EPSC model, or other self-consistent codes [39], can describe reasonably well the evolution of the grain orientation (texture). This is because texture evolution is not very sensitive to the orientation anisotropy of the stress states, at least for cubic materials. However, accurate prediction of the intergranular stress still remains a challenge for these models. A major difficulty there is the lack of appropriate descriptions for the grain-to-grain interactions, which are closely connected to the number of active slip systems and the hardening behavior of each slip system. Although a complex hardening matrix can be defined within the framework of the EPSC model to account for the interactions between slip systems [40], the number of required parameters to carry out the simulation is

just too large. Another limitation with the EPSC model is that not all grains with different orientations fully comply with the self-consistent state due to the existence of dislocations or other defaults near the grain or phase boundaries. Hence it is still a challenge for these models to simulate the detailed microstructures and substructures produced in the large plastic deformation regime. In fact, the above-mentioned two limitations also apply to finite element based simulations of the inter-granular stress. As a consequence, there has been no report comparing experimental lattice strains and calculations by numerical models in the large plastic deformation regime. In materials where phase transformation occurs during deformation, the inter-granular stress becomes even more complex, especially when the transformation is selective with respect to the crystallographic axes. In this regard, the experiment data presented in this paper should provide a useful guide for the development of numerical models for simulation of deformation behaviors and phase transformation of polycrystalline materials subjected to a moderate or large degree of deformation.

5.3. Residual stress after recovery

Understanding the change of residual stress during recovery is an important step in determining the influence of residual stress on recrystallization texture [28]. The change of residual stress during annealing can be considered into two parts. First, a new phase-stress of thermal origin develops. Second, the orientation anisotropy of the residual stress in both phases are reduced.

The development of phase-stress after annealing can be explained by the mismatch of thermal expansion coefficients between the α and γ phases. When the cold-rolled sample is heated to high temperature (500°C), recovery occurs in both γ and α phases. As a consequence, the phase-stresses produced by cold rolling are largely relaxed at high temperature. When the sample is cooled down, thermal residual stress is introduced due to the different coefficients of thermal expansion for the two phases. As the thermal expansion coefficient for the γ phase (18.0×10^{-6} K^{-1}) is higher than that for the α phase (12.4×10^{-6} K^{-1}) [41], the γ phase will show a tensile phase-stress after cooling to room temperature, whereas a compressive phase-stress is produced in the α phase. Note that the phase-stresses in the annealed sample are almost bi-axial, with $\sigma_{11} \approx \sigma_{22}$ and $\sigma_{33} \approx 0$. This result confirms that the initial phase-stress due to cold rolling was essentially eliminated by annealing at 500°C. The small σ_{33} in the annealed sample suggest that upon cooling, phase-stresses were allowed to develop within the plane but not in the normal direction, which may be due to the specific microstructures, i.e. the pancaked grains of both the α and γ phases.

The change of orientation anisotropy of residual stress during annealing is far more complex than that of the phase-stress. In the α phase, all Δ_{ij} values are less than 0.3. In the γ phase, however, while Δ_{11} and Δ_{22} are reduced to below 0.3, a residual value of 1.2 was found for Δ_{33}. This observation contrasts with that in the cold-rolled sample, where the highest anisotropy was always found in the rolling direction. The large residual value for Δ_{33} means that a significant amount of intergranular stress still exists in the normal direction and the recovery in the γ phase is not complete. Indeed, analysis of the peak shape profile shows that after annealing the Bragg peak widths in the α phase are drastically reduced, while peak widths in the γ phase decrease only slightly, which means that the degree of recovery is higher in α than in γ. The change of Δ_{ij} values before and after annealing is consistent with this picture. For example, in the rolling direction, Δ_{11} changes from 7.0 to 0.1 in the α phase. Meanwhile in the γ phase, Δ_{11} changes from 4.8 to 0.3. The large residual value of Δ_{33} in the γ phase is not surprising in view of the elongated grain microstructures generated by cold rolling. By virtue of force balance, residual stress in the γ phase is also relaxed at the same time when the recovery takes place in the α phase. The elongated grains lead to more surface areas in the plane, allowing σ_{11} and σ_{22} to relax more readily than σ_{33}. All things considered, it appears that the recovery in this two-phase material is driven by the α phase.

Analysis of the change in residual stress values before and after annealing indicates that in the γ phase, the recovery is more or less uniform for

major texture components. This is, however, not the case in the α phase, where the order of easy recovery orientations was found to be $\{1\,1\,1\}\langle 1\,1\,2\rangle$, $\{1\,1\,1\}\langle 1\,1\,0\rangle$, $\{1\,1\,2\}\langle 1\,1\,0\rangle$ and $\{0\,0\,1\}\langle 1\,1\,0\rangle$. Fig. 10 compares the change of residual stress for the α phase, calculated from the SODF determined for the cold-rolled and annealed samples, respectively, with the release of stored energy in IF steel during recovery [42]. The release of stored energy for different texture components in the IF steel was derived from the measurements of peak broadening using neutron diffraction. It can be seen that, despite the differences in chemical composition between the two materials, the change of residual stress in the α phase is in reasonable agreement with the release of stored energy in IF steel. Thus, it appears that high temperature relaxation of residual stress in cold-rolled steel is closely related to the release of stored energy.

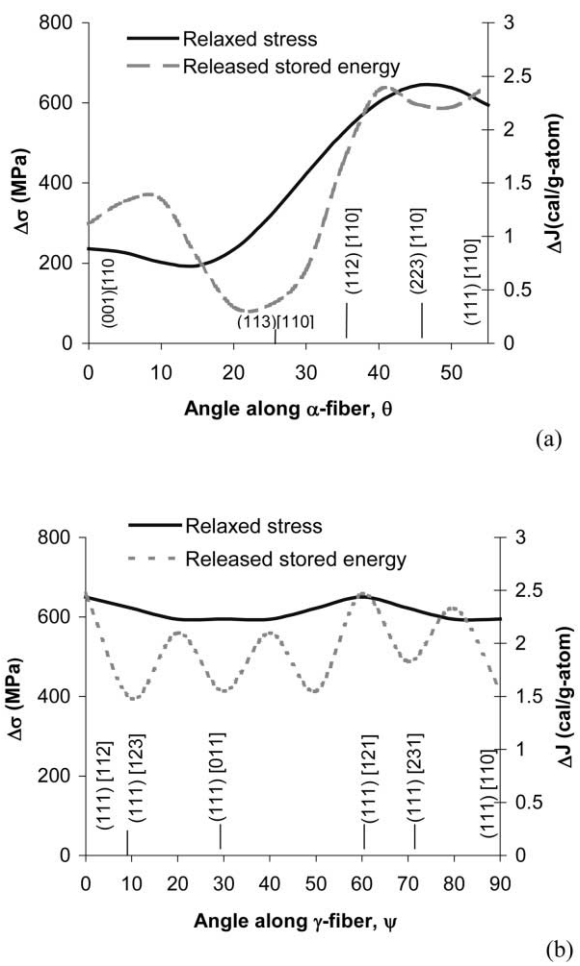

Fig. 10. Comparison of the change of residual stress in the α phase with the release of stored energy in IF steel [42].

Finally a few remarks can be made about the SHA method. The present study demonstrates that SHA is a powerful method for experimental determination of the grain-orientation-dependent residual stress in materials. With this method, the SODF was constructed directly from the experimental data.

It should be pointed out, however, that the SHA method gives only the mean stress field over all grains with equivalent orientations since neutron diffraction measures the average strain of all grains satisfying the Bragg condition within the scattering volume, usually on the order of ~mm^3. Nevertheless, as the present study shows, the SODF determined from neutron diffraction experiments contains rich information for understanding the mechanical behaviors on the scale of the grain size. This is because the SODF, as a statistical means, gives explicitly the correlation between the mean stress field and the grain orientation. Moreover, the stress at the level of a grain depends not only on the crystal structure and microstructure, but also on the elastic and plastic anisotropy of a single crystal and the thermo-mechanical history. All the information is contained in the SODF. For these reasons, the experimentally determined SODF has proven to be a useful tool for understanding the interactions between grains.

The SODFs presented in this paper should probably be characterized as "low-resolution" because the measurement grid ($10° \times 10°$) is coarse and only strain pole figures for a few low index reflections were measured. These limitations prevent the expansion of the series coefficients of the SODF to high orders unless a constraint condition is used. In this study, a self-consistent scheme was used as a weak constraint condition in order to find a reasonable solution amongst a variety of possible ones, all of which are in agreement with the measured diffraction strains. This condition is not necessary when a large number of reflections are meas-

ured (for example, at a pulsed neutron source) using a fine measurement grid.

6. Summary

In this study, neutron diffraction was used to investigate the grain-orientation-dependent residual stress in cold-rolled stainless steel. The material consists of two-phases, 62 vol% γ and the rest α. The residual stress in each sample was determined using the spherical harmonic analysis by constructing the SODF from the measured strain pole figures. In the cold-rolled sample, a high degree of grain-orientation-dependent stress anisotropy was observed in both γ and α phases. For some of the specimen directions, the local residual stresses within a grain vary widely, from tension to compression, and its magnitudes can be much larger than the phase-stress. For this material, stress analysis by the conventional method (e.g., "d-space" vs $\sin^2\Psi$) fails completely and should not be used. The experimentally determined inter-granular and phase stresses are consistent with the selective transformation that occurred during deformation by cold rolling.

Annealing at 500°C leads to a re-distribution of the residual stress. First, new phase-stresses develop as a result of the thermal expansion mismatch between the α and γ phases. Second, recovery occurs during annealing which reduces the orientation anisotropy of residual stress in both phases. In the α phase, the recovery is fast and almost completely eliminated the orientation stress anisotropy or inter-granular stress found in the cold-rolled condition. The recovery in the γ phase is slow and incomplete. In particular, a significant amount of inter-granular stress in the γ phase still exists along the normal direction. These observations suggest that the overall recovery behavior in this two-phase material is driven by the recovery in α phase and the cold rolling microstructures also play a role. For the α phase, the change of residual stress during recovery appears to be closely related to the release of stored energy. Further investigations (e.g., with different annealing temperature and annealing time) are necessary in order to develop a thorough understanding of the fascinating recovery dynamics.

Acknowledgements

The authors are grateful to Mr. B. Trostell for technical assistance with the neutron diffraction measurements, and Mr. L.E. Karlsson and Ms. J. Eriksen for preparation of the neutron diffraction samples. This research was supported in part by an appointment (YDW) to the Oak Ridge National Laboratory Postdoctoral Research Associates Program administered by the Oak Ridge Institute for Science and Education and Oak Ridge National Laboratory. Oak Ridge National Laboratory is managed by UT-Battllee, LLC, under contract DE-AC05-00OR22725 for the U.S. Department of Energy.

References

[1] Behnken H, Hauk V. Steel Research 1996;67:423.
[2] Brakman CM. J. Appl. Cryst. 1983;16:325.
[3] Brakman CM, Penning P. Acta Cryst. A 1988;44:163.
[4] Marion RH, Cohen JB. Adv. X-ray Anal. 1975;18:466.
[5] Noyan IC, Schadler LS. Metall. Mater. Trans. A 1994;25:341.
[6] Schuman C, Humbert M, Esling C. Z. Metallk. 1994;85:559.
[7] Matthies S, Humbert M. J. Appl. Cryst. 1995;28:254.
[8] Wang YD, Lin Peng R, McGreevy R. Scripta Mater. 1999;41:995.
[9] Van Acker K, van Houtte P, Aernoudt E. In: ICOTOM-11, vol. 2. 1996. p. 1461.
[10] Clausen B, Lorentzen T, Leffers T. Acta Mater. 1998;46:3087.
[11] Pang JW, Holden TM, Mason TE. Acta Mater. 1998;46:1503.
[12] Daymond MR, Tomé CN, Bourke MAM. Acta Mater. 2000;48:553.
[13] Dawson P, Boyce D, MacEwen S, Rogge R. Metall. Mater. Trans. A 2000;31:1543.
[14] Raabe D. Acta Mater. 1997;45:1137.
[15] Goodchild D, Roberts WT, Wilson DV. Acta Metall. 1970;18:1137.
[16] Kocks UF, Tomé CN, Wenk HR. Texture and anisotropy. Cambridge University Press, 1998.
[17] Margulies L, Winther G, Poulsen HF. Science 2001;291:2392.
[18] Ice GE, Larson BC. Adv. Eng. Mat. 2000;2:643.
[19] Delaire F, Raphanel JL, Rey C. Acta Mater. 2000;48:1075.
[20] Nugent EE, Calhoun RB, Mortensen A. Acta Mater. 2000;48:1451.
[21] Raabe D, Sachtleber M, Zhao Z, Roters F, Zaefferer S. Acta Mater. 2001;49:3433.

[22] Hoffmann J, Neff H, Scholtes B, Macherauch E. In: Proceedings of the 5th Risö International Symposium on Metallurgy and Material Science. Roskilde, Denmark: Risö National Laboratory; 1984. p. 595.
[23] Perlovich Y. In: Proceedings of the 15th Risö International Symposium on Material Science. Roskilde, Denmark: Risö National Laboratory; 1994. p. 445.
[24] Wang YD, Lin Peng R, McGreevy R. In: ICOTOM-12, vol. 1. 1999. p. 553.
[25] Wang YD, Lin Peng R, Zeng XH, McGreevy R. Mater. Sci. Forum 2000;347-349:66.
[26] Behnken H. Mater. Sci. Forum 2000;347-349:273.
[27] Bunge HJ. Mater. Sci. Forum 1994;157-162:13.
[28] Park YB, Lee DN, Gottstein G. Acta Mater. 1998;46:3371.
[29] Wang YD, Xu JZ, Liang ZD. Textures and Microstructures 1996;26-27:103.
[30] Wang YD, Lin Peng R, McGreevy RL. Phil. Mag. Lett. 2001;81:153.
[31] Bunge HJ. Z. Metall. 1965;56:872.
[32] Roe RJ. J. Appl. Phys. 1965;36:2024.
[33] Eshelby JD. Proc. Roy. Soc. Lond. A 1957;241:376.
[34] Ledbetter HM. Phys. Stat. Sol. A 1984;85:89.
[35] Simmons G, Wang H. Single crystal elastic constants and calculated aggregate properties: a handbook. MIT Press, 1971.
[36] Clausen B, Lorentzen T, Bourke MAM, Daymond MR. Mater. Sci. Eng. A 1999;259:17.
[37] Pang JW, Holden TM, Wright JS, Mason TE. Acta Mater. 2000;48:1131.
[38] Turner PA, Tomé CN. Acta Metall. 1994;42:4043.
[39] Molinari A, Canova GR, Ahzi S. Acta Metall. 1987;35:2983.
[40] Tóth LS. In: ICOTOM-11, vol. 1. 1996. p. 347.
[41] Harjo S, Tomota Y, Ono M. Acta Mater. 1999;47:353.
[42] Rajmohan N, Hayakawa Y, Szpunar JA, Root JH. Acta Mater. 1997;45:2485.